Materials Today Physics 16 (2021) 100307

Contents lists available at ScienceDirect

Materials Today Physics

journal homepage: https://www.journals.elsevier.com/materials-today-physics

Anionic conduction mediated giant *n*-type Seebeck coefficient in doped Poly(3-hexylthiophene) free-standing films

M. Bharti [a, b, *], A. Singh [a, **], A.K. Debnath [a], A.K. Chauhan [a], K.P. Muthe [a], S.K. Gupta [a], K. Marumoto [c], T. Mori [d, ***], D.K. Aswal [a, e]

[a] Technical Physics Division, Bhabha Atomic Research Centre, Trombay, Mumbai, 400085, India
[b] All India Jat Heroes' Memorial College, Rohtak, 124001, Haryana, India
[c] Division of Materials Science, University of Tsukuba, 1-1-1Tennodai, Tsukuba, Ibaraki, 305-8573, Japan
[d] National Institute for Materials Science (NIMS), International Center for Materials Nanoarchitectonics (WPI-MANA), Namiki 1-1, Tsukuba, Japan
[e] CSIR-National Physical Laboratory, New Delhi, 110012, India

ARTICLE INFO

Article history:
Received 21 August 2020
Received in revised form
20 October 2020
Accepted 21 October 2020
Available online 26 October 2020

Keywords:
Thermoelectric
Conducting polymers
Poly(3-hexylthiophene)
Ionic conduction
Free-standing
Seebeck coefficient
n-type
Soret effect
Intermittent heat conversion
Thermodiffusion

ABSTRACT

The present work demonstrates a totally radical change in conduction nature from typical *p*-type to *n*-type through ionic transport in $FeCl_3$ doped free-standing poly(3-hexylthiophene) (P3HT) films. The thermodiffusion of Cl^- ions generated a giant negative Seebeck coefficient (~2.7 mV/K) and a moderately high electrical conductivity (~1 S/cm); an unprecedented level in polymers. A thermoelectric power generator fabricated using these P3HT films delivered an output electrical power of 25 μW with open circuit voltage of 128 mV for a ΔT of 46 °C. Though continuous operation reduced the output power due to inability of the ions to pass through the interface between doped P3HT and metallic contact, yet the generated voltage was found to be quite stable over a period of 1 h under load. With such a high *n*-type Seebeck coefficient, free-standing P3HT films show a great potential for energy harvesting from intermittent heat sources as well as in supercapacitor charging for futuristic energy storage devices.

1. Introduction

Thermoelectricity that converts ambient heat into useful power has attracted the attention of researchers worldwide as a promising energy harvesting technology. A lot of focus has been exerted to develop efficient thermoelectric (TE) materials that can harness/recover room temperature heat [1,2]. In this view, conducting polymers are being explored as the new class of energy storing or thermoelectric materials over recent years. Their solution processability, flexibility, cheaper cost of processing along with already shown potential in flexible electronics, are advantages for organic thermoelectric devices [3–8]. However, for an efficient thermoelectric material, a parameter known as thermoelectric figure-of-merit (ZT) should be high. ZT is given by $\alpha^2\sigma T/\kappa$; therefore, to have high ZT at a particular operating temperature T, a high Seebeck coefficient (α), high electrical conductivity (σ), and low thermal conductivity (κ) are desirable. Unfortunately, these three parameters α, σ, and κ are interdependent and need to be decoupled for a high thermoelectric efficiency [9]. Therefore, conducting polymers with intrinsic low thermal conductivity and amenability towards doping show good possibility to manipulate these parameters through variation in carrier concentration and charge carrier mobility. In fact, due to facile tuning of electrical conductivity, the majority of the initial research on conducting polymers has remained focused on its improvement of electrical transport; rather than being concentrated on improving the Seebeck coefficient which is generally quite low for conducting polymers [10–13].

* Corresponding author. Technical Physics Division, Bhabha Atomic Research Centre, Trombay, Mumbai, 400085, India.
** Corresponding author.
*** Corresponding author.
E-mail addresses: meetubharti@yahoo.com (M. Bharti), asb_barc@yahoo.com (A. Singh), mori.takao@nims.go.jp (T. Mori).

https://doi.org/10.1016/j.mtphys.2020.100307

However, it has been recently reported that ionic transport may be utilized in addition to the traditional electronic thermoelectric (TE) effect to boost the magnitude of TE voltage [10–12]. For ionic conductors, it has been demonstrated that a large thermally-induced voltage of the order of few mV/K can be generated. But, on the other hand, poor charge carrier mobility of ions keep the electrical conductivity of typical ionic conductors much lower (by several orders of magnitude) as compared to conventional TE materials that are driven by electronic transport. One of the classic examples of a conducting polymer which exhibits high Seebeck coefficient due to ionic contribution is PEDOT-PSS-PSSNa [11,12,14]. However, most of the thermoelectric studies of PEDOT-PSS have focussed on the manipulation of electronic transport for improving its performance; mainly through the removal of the extra dopant PSS. Because in a commercially prepared PEDOT-PSS, the ratio of PEDOT to PSS is around 0.26, and considering an optimum doping level of 33%, only about 10% of PSS will balance the positive charge in PEDOT; while the rest of the PSS ions will remain present as mobile cations and restrict the facile motion of the charge carriers due to localized electric field. Therefore, addition of secondary dopants such as dimethyl sulphoxide (DMSO) or ethylene glycol (EG) which can remove extra PSS results in enhancement of electronic conductivity. On the other hand, if PSSNa (a salt which functions as an electrolyte) is added to PEDOT-PSS, its ionic conductivity can be enhanced to a great extent [11,12,14]. However, the magnitude of the ionic conductivity is much lower than electronic conductivity due to low mobility of ions. But such a conducting polymer usually exhibits large Seebeck coefficient due to migration of heavy positively charged ions from the hot-end to cold-end; and this thermo-diffusion of ions is known as the Soret effect [10–12,15,16]. Therefore, if anyhow, ionic conduction to improve the Seebeck coefficient and electronic conduction to improve the electrical conductivity can be channelized together, the three parameters (α, σ, κ) can be more easily optimized to design and develop an efficient organic thermoelectric material [13]. Such concept of optimizing both ionic and electronic transport finds its support by Ouyang et al. who reported recently that combination of polyelectrolytes and conducting polymers can be used to optimize the power factor ($\alpha^2\sigma$). Ouyang et al. demonstrated that ionic conduction in the PSSH layer of a PSSH/PEDOT-PSSS sample creates an energy barrier that improves the overall Seebeck coefficient by the energy filtering effect [14]. However, in order to achieve dominance of ionic conduction in TE properties, the electronic conductivity of materials certainly gets compromised.

In the present study, poly(3-hexylthiophene) (P3HT) has been selected owing to several merits such as ready availability, ease of processing from solution, and promising electrical properties arising from a highly crystalline microstructure [17–22]. Moreover, its advantage of being soluble in common organic solvents, makes it suitable for various solution-processed techniques like drop-casting, spin/bar-coating *etc*. Many research groups have reported improvement in thermoelectric properties of P3HT by simple means of doping or through incorporating carbon nanotubes (CNTs)/inorganic components [22–28]. For instance, Crispin et al. reported three orders enhancement in power factor from approximately 10^{-10} W/mK^2 to 1.4 × 10^{-7} W/mK^2 through optimizing the negatively charged counter-ions as dopants [18]. Similarly, through incorporation of ferric salt of triflimide $TFSI^-$ ($(CF3SO2)2N^-$) power factor ~20 μW/mK^2 was obtained and it had been one of the highest ever reported power factors for P3HT [19]. He et al. incorporated Bi_2Te_3 nanopowder in P3HT matrix and demonstrated that organic/inorganic interface can be created to enhance Seebeck coefficient and power factor via energy filtering effect [20]. But, most of the work in polymers including P3HT has been reported with *p*-type polaronic conduction only, even though it has been found that utilizing ionic transport may result in higher Seebeck coefficients [15].

Moreover, it is essential to develop an '*n*-type' polymer, for conventional design of thermoelectric modules which require both *p*- and *n*- TE elements. Recently, *n*-type ionic behaviour has been observed in a polymer gel electrolyte yet no '*n*-type' ionic thermoelectric conducting polymer showing Soret effect has been reported so far. We have been able to achieve such a rare *n*-type ionic conduction in P3HT films in the present work. Doping by ferric chloride generated chloride anions whose thermodiffusion caused an enormous increase in *n*-type Seebeck coefficient (~−2729 μV/K at 70 °C). In fact, P3HT is the only polymer other than PEDOT:PSS which exhibits ionic conduction, which is not humidity dependent. These films exhibiting anionic conduction can be a potential alternative to those conducting polymers/polymer electrolytes where ionic transport is determined by the electrolyte which is mostly water or salt, and thus, can have degraded performance when subjected to a large temperature gradient. Moreover, these substrate-adherent P3HT films, on doping, attained the free-standing motif. In search of the plausible mechanism behind huge *n*-type Seebeck coefficient, we propose that ionic conduction in $FeCl_3$ arises due to formation of $(Fe_2Cl_5)^+$ and $(Fe_2Cl_7)^-$ ionised species in equilibrium with bitetrahedral Fe_2Cl_6 molecules as supported by Tosi et al. [23] The movement of negatively charged Cl^- ions *i.e.* anions from $(Fe_2Cl_7)^-$ resulted in *n*-type conduction of P3HT films. In order to investigate the use of these P3HT films for real applications, we designed a prototype thermoelectric power generator which delivered an output electrical power of 25 μW with open circuit voltage of 128 mV for a ΔT of 46 °C. However, inability of ions to find passage through the interface between doped P3HT and metallic contact will not allow generating a constant electrical power under continuous operation (i.e. under constant temperature gradient) but such thermo-diffusion of ions can produce a large constant voltage to be exploited for heat flux sensing or temperature measurements [15]. In fact, the reported P3HT films having a huge *n*-type Seebeck coefficient can be a promising material for intermittent heat conversion/supercapacitor charging; and being free-standing would realize flexible and wearable energy harvesting.

2. Experimental procedures

2.1. Fabrication of P3HT samples

For preparation of films, P3HT powder, procured from Sigma Aldrich, was dissolved in ortho-dichlorobenzene to make a solution of 35 mg/ml concentration, which was homogenised for 2 h using a magnetic stirrer. The solution was drop-casted on Kapton (polyimide) substrates to deposit P3HT films. The films were kept for air-drying and annealed for 15 min at 70 °C in an oven. The resulted undoped films were found to be golden in colour and highly adherent to the substrate. Thickness of these substrate-adherent films was found to be ~10 μm and estimated by determining the mass of the deposited film and density of P3HT. While, for doping of ferric chloride ($FeCl_3$) into the P3HT matrix, the annealed films were dipped for 7 min in a $FeCl_3$ solution in Nitrobenzene (procured from Sigma Aldrich) with three different concentrations i.e. 25, 50 and 75 mM of $FeCl_3$ (and the films doped using 25, 50 and 75 mM of $FeCl_3$ solution are named as F25, F50 and F75 respectively in the later part of the manuscript). After dipping in $FeCl_3$, golden colour of the pristine films at once changed to (shining) blackish which clearly indicated that doping had taken place. Also, after getting doped, the films themselves peeled-off from the substrates and achieved a free-standing motif which had a very good mechanical strength (could be bent by 180° for many times). Thickness

of the doped films was estimated 12 μm and such enhancement in comparison to thickness of pristine films can be attributed to fluffiness due to intercalation of dopants. The mechanical strength of the doped P3HT films is revealed through the photographs of the films taken during the bending process, and also at the time of making live measurements for the resistance of films during bending experiment. The photographs along with the description about the films' behaviour during bending process are shown in Figure S1 of supplementary information. In fact, we found that pristine solution could be deposited on any large-area substrate such as a glass slide (7.5 cm × 2.5 cm) to achieve free-standing film of desirable dimensions. Schematic of the process describing steps of samples (films) preparation along with photographs of actual films is shown in Fig. 1.

2.2. Films' characterizations

The films were characterized using various techniques. The change in morphology was investigated through Atomic Force Microscopy using Solver Next (NT-MDT) as well as by scanning electron microscope (Model: Vega 3, MV 2300/T40, Tescan). While chemical nature of films was studied by X-ray photoelectron spectroscopy (XPS) carried out using Mg-Kα (1253.6 eV) source and DESA-150 electron analyzer (Staib Instruments, Germany). A high resolution XPS spectrum for each element was recorded by taking an average of 15 scans. The binding-energy scale was calibrated to C-1s line of ~284.6eV and Gaussian distributions functions were used to fit the XPS peaks. In addition, while fitting the XPS data having 2 or more peaks, the boundary condition of full-width at half maximum (FWHM) was applied for each of the peaks. The samples were also characterized by Fourier-transform infrared spectroscopy (Bruker 80V) and the Raman spectroscopy measurements were carried out using LABRAM-1, ISA micro-Raman spectrometer with 632.8 nm line of He-Ne laser for excitation. Room-temperature Hall measurements were done for estimation of carrier concentration, type of carriers, and mobility in Vander Pauw four-probe configuration geometry. These measurements were carried out in a standard set-up (ECOPIA, Model No. HM55000) at applied magnetic field and DC current of 0.5 T and 100 μA respectively. The lab-made experimental set-up was used to measure temperature-dependent thermoelectric properties of samples. In this set-up, four-probe electrical conductivity and Seebeck coefficient can be simultaneously measured in a temperature controlled oven. Eurotherm PID temperature controller (Model No.: 2416) was used to maintain the oven temperature with an accuracy of ±0.5 °C. Hot- and cold-end temperatures of the samples were measured using platinum resistors (Pt-100). Keithley nanovoltmeter (Model No. 2182) was used for measurement of Seebeck voltage and Keithley source meter 2400 was used to measure four-probe electrical conductivity. Electrical contacts, for these measurements, were made on the sample surface with the help of silver wires (of diameter ~200 μm) that were attached through high conductivity silver paint (Electrolube UK make). The prepared free-standing films were also characterized by electron spin resonance (ESR) technique by using JEOL JES-FA200 spectrometer at room temperature. The observed *g*-value was determined from the resonance field of ESR signal and the peak-to-peak line width of the field-induced signal by applying magnetic field perpendicular to the films' surface.

3. Results and discussion

Temperature dependent thermoelectric properties (i.e. electrical conductivity, Seebeck coefficient and power factor) have been measured for both the undoped and doped films and results are shown in Fig. 2. The films named as F25, F50 and F75 show three different concentrations of the doping content i.e. 25, 50 and 75 mM of $FeCl_3$ solution. Undoped (pristine) films showed the lowest electrical conductivity of ~3.6×10^{-5} S/cm at room temperature that increased slowly with the temperature. However, electrical conductivity increased by 2-5 orders of magnitude with doping in case of F25 and F50 films but reduced on further doping i.e. for F75 films as shown in Fig. 2(a). The Seebeck coefficient (α) for undoped films was found to have a small positive value of ~55 μV/K (at 70 °C); thus, indicating *p*-type conductivity. On the other hand, films doped with $FeCl_3$ exhibited a very large negative α (in the range from 1 to 15 mV/K) indicating predominantly negative-ion conductivity as such high values have only been reported in case of ionic polymer conductors [10–14].

Seebeck coefficient for these doped films showed systematic enhancement with the $FeCl_3$ concentration with a very large (negative) value of $\alpha \sim -14$ mV/K for F75 films at room temperature. However, value of α began to decrease with increase in temperature in case of F75 films. Whereas, both the F25 and F50 samples exhibited a reasonably high negative value of α with weak temperature dependence (shown in Fig. 2(b)). This strong temperature dependence of F75 films in comparison to both F25 and F50 films can be attributed to different concentration of the doping content in these films. F75 films being heavily doped have large numbers of polarons with positive charge; also confirmed by ESR measurements discussed in Fig. 4(e and f). Moreover, heavy doping in these F75 films perhaps results in better connected network of $FeCl_3$

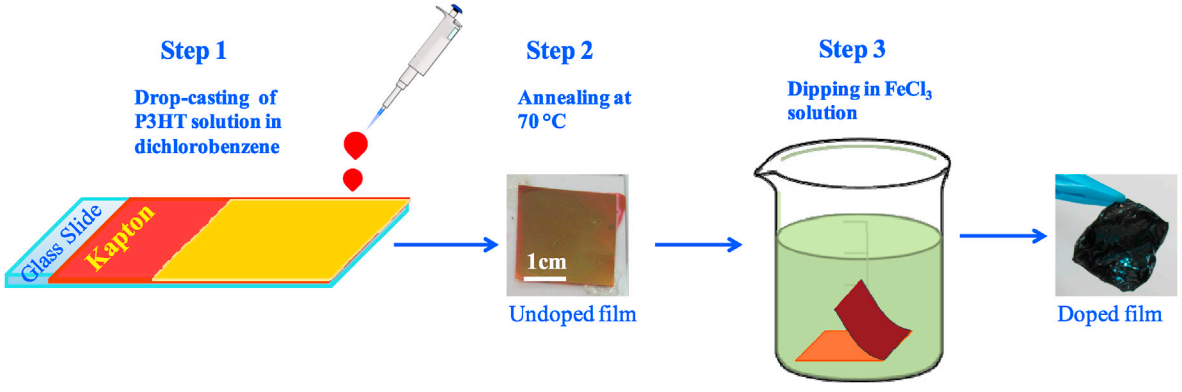

Fig. 1. Schematic showing the procedure for synthesis of P3HT films along with the actual photographs of both the undoped (pristine and substrate-adherent) and doped (free-standing) films.

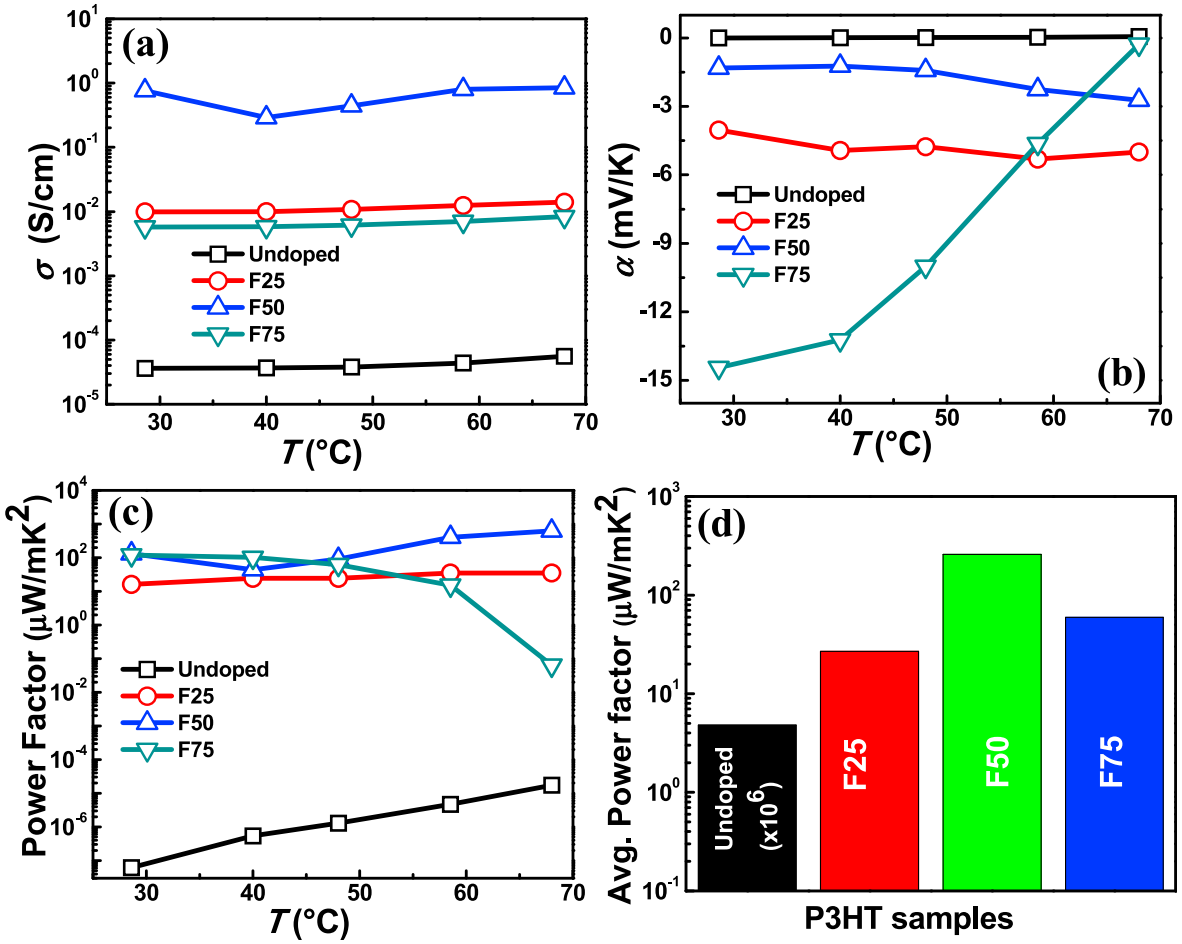

Fig. 2. Temperature dependent thermoelectric properties of P3HT films: (a) Electrical conductivity; (b) Seebeck coefficient; and (c) Power factor; (d) Comparison of average power factor for different films (Note that power factor values for undoped samples have been multiplied with 10^6).

domains and thus, can provide high mobility path to anions. Therefore, with the increase in temperature, more numbers of polarons and bipolarons will reach the cold-end in case of heavily doped F75 and cancel out the negative Seebeck voltage generated by the anions. The strong temperature dependence of the F75 film was reproduced for a different batch (as shown in Figure S4 of the supplementary information). We have provided a qualitative explanation for this peculiar temperature dependence in case of heavy doping. However, such behaviour is interesting and should be elucidated further in future works. On the other hand, F25 and F50 having relatively less concentration of the dopants, therefore, exhibited negligible dependence on temperature.

In fact, Seebeck coefficient of doped P3HT samples is found to be much higher than that of conventional inorganic thermoelectric materials such as Bi_2Te_3 and to the best of our knowledge, such a high negative Seebeck coefficient has not been reported yet for pure organic thermoelectric materials with polaronic transport. We would like to point out that a similar absolute value (but typically positive) of Seebeck coefficient ~14 mV/K due to cationic conduction has been reported recently, in case of the hybrid films of poly(3,4-ethylenedioxythiophene)-tosylate (PEDOT-Tos) and carbon nanotubes [13,24]. However, the doped P3HT films reported here, exhibited a very high power factor $\alpha^2\sigma$ also (shown in Fig. 2(c)) because of the cumulative effect of high electrical conductivity and Seebeck coefficient. Average values of power factors for different films have been compared in Fig. 2(d) and it was observed that 50 mM samples showed the highest value of $\alpha^2\sigma$ ~628 μW/mK^2 (at 70 °C). Such a large and negative Seebeck coefficient obtained in case of doped films indicates that majority of the conduction occurred by negative ions. To further confirm the type of conduction as well as to estimate carrier concentration of P3HT films, both the F50 (i.e doped) and undoped samples were characterized by impedance spectroscopy and Hall's measurements. The results of Hall measurements are given in Table 1. The undoped films show extremely low *p*-type carrier concentration (of ~4.5 × 10^{16} cm^{-3}) and low mobility values that are in agreement with those reported in literature [25,29]. While, for doped films Hall measurement showed that the carriers' concentration increased by nearly four orders of magnitude with doping and also confirmed their *n*-type conduction.

It should be noted that ionic conduction in $FeCl_3$ has also been reported earlier due to formation of $(Fe_2Cl_5)^+$ and $(Fe_2Cl_7)^-$ ionised species in equilibrium with bitetrahedral Fe_2Cl_6 molecules [23]. On a similar note, conduction in case of $FeCl_3$ doped P3HT films has been attributed to the hopping of Cl^- ions from $(Fe_2Cl_7)^-$. Though charge carriers in the doped films are expected to be predominantly negative ions yet some electronic (*p*- or *n*-type) conduction could also exist. This predominance of ionic conduction was further confirmed by the impedance spectroscopy, whereas electron spin resonance and Kelvin probe data discussed ahead indicated that there existed a small (negative) electronic contribution also. However, some more studies are required to determine the detailed conduction mechanism but the results as obtained show reasonable agreement with this proposition. Impedance spectroscopy

Table 1
Results of Hall measurement (carried out at 300 K) for P3HT films.

Sample details	Conductivity (S/cm)	Carrier concentration (cm^{-3})	Charge carrier mobility (cm^2/Vs)	Type of conduction
Undoped films	3.6×10^{-5}	4.5×10^{16}	0.005	*p*-type
Doped, F50 films	0.76	2.6×10^{20}	0.018	*n*-type

data for both undoped and F50 films are shown in the form of Nyquist plots in Fig. 3. In case of undoped films, one can see a segment of a semi circle in the high frequency region and a small linearly rising lower frequency component. Linear low frequency component is attributed to the electrode polarization effects. Whereas for doped films, a depressed semicircle at high frequencies, a segment of semicircle at mid frequencies, and a linearly rising lower frequency component is observed. Size of semicircle at mid frequencies suggests dominance of ionic conduction [12,30,31]. Finally, the results of impedance spectroscopy were analyzed by fitting them to equivalent circuits (shown in the insets of Fig. 3) and a summary of the results is given in Table 2 [12,31,32]. It can be concluded that doped $FeCl_3$ served as an active material that is dispersed into the P3HT matrix and therefore, functioned simultaneously as the conductor of chloride anions (Cl^-) and electronic charge as supported by Balsara et al. also [31]. In fact, thermodiffusion of Cl^- ion through the P3HT matrix has also been confirmed by the XPS data of hot- and cold-ends of the sample and discussed in S2 section of the supplementary information.

In addition, dopant $FeCl_3$ served as a connecting material when inserted between the polymer chains and supported hopping of charge carriers; but at the same time disturbed the aligned structure making it the amorphous one (as confirmed by XRD analysis also) which in turn would reduce electronic conductivity. The results of impedance spectroscopy clearly exhibit that conduction in doped samples is predominantly ionic (about 500 times that of electronic contribution) as expected.

The results of surface morphology and crystalline structure of films as studied by AFM and XRD are shown in Fig. 4(a). The AFM images reveal that undoped films have granular morphology with typical RMS surface roughness of ~12.1 nm, and doping with $FeCl_3$ did not cause any significant change in this surface roughness (shown in the image of sample F50). However, the SEM images shown in Figure S3 of the supplementary information revealed that undoped films were quite smooth in comparison to the doped films. XRD spectrum for undoped films shows three sharp diffraction peaks at 5.3°, 10.8° and 16.4°, (corresponding respectively to *100, 200* and *300* planes) which indicate that films are predominantly crystalline with edge-on stacking of P3HT planes [33,34]. Whereas, a broad peak seen at 2θ ~21.8° indicates a small amorphous component [35]. The analysis of XRD data for undoped films reveals that polymer chains are highly oriented in a stacked structure (due to π-π interaction of overlapping aromatic rings) with out-of-plane spacing as 16.7 Å (zipper like connection of side alkyl chains) [19,34]. While, the XRD data of doped films showed a broad and small (*100*) peak at lower 2θ (~4.9° and FWHM~0.97°) and a much larger amorphous component. Reduced 2θ value for (*100*) peak indicates increased out-of-plane stacking distance (~18.7 Å) and such an increase of interplanar spacing occurred due to intercalation of ions [33,34,36,37]. However, very low electronic conductivity exhibited by the doped films has been attributed to the amorphous structure that inhibited movement of carriers. On the other hand, high ionic conductivity has been explained on the basis of flexible backbone of the amorphous structure as already reported in a study on '$FeCl_3$ doped HPMC films' [38]. We would like to mention that if the doped films were annealed at temperature >70 °C or kept in air for a long time (greater than 3 months), they started exhibiting usual *p*-type conduction and positive Seebeck effect. To understand this change in conduction nature, XRD of a doped film which had prolonged air exposure (>3 months) was carried out and the obtained data is given in an inset of Fig. 4(a). From the inset, it is clear that (*100*) diffraction peak at 2θ ~5.1° is very sharp (FWHM ~ 0.49°) similar to that observed in case of undoped films (2θ~5.3° and FWHM ~0.47°); but the broad peak at 2θ ~21.8° related to the amorphous structure got depressed in intensity. This reveals that these doped but air-exposed (for long duration >3 months) films are crystalline in nature and show usual hole polaron conduction; but at the same time it can be concluded that amorphous structure is necessary for exhibiting negative ion dominated large Seebeck effect.

The typical UV-vis-NIR absorption spectra of both undoped and F50 films are shown in Fig. 4(b). It is observed that intensity of π-π* transition peak at 525 nm gets significantly reduced for doped films whereas new intense absorption bands appear at 790 nm and in NIR region (>1400 nm). These bands may be attributed to formation of polarons and bipolarons through doping [39–41]. However, even after formation of polarons and bipolarons, electronic conduction remained poor mainly due to amorphous structure. This formation of polarons/bipolarons has also been confirmed by the ratio Avg Spin No./Mass as estimated by the ESR measurements that

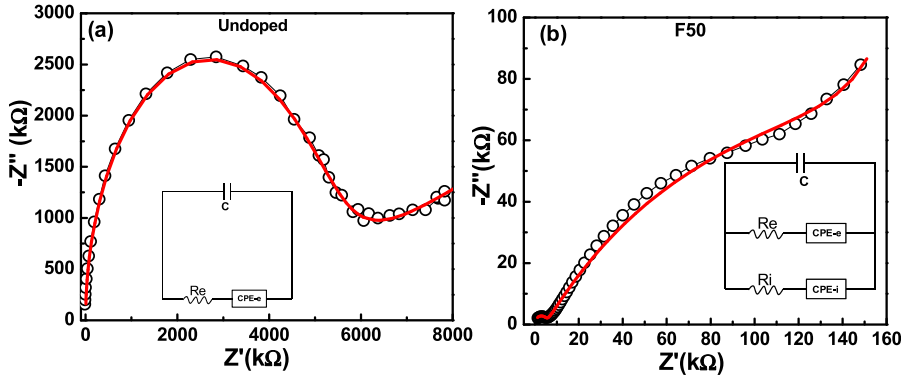

Fig. 3. Nyquist plots for (a) Undoped; and (b) F50 films (Insets show equivalent circuits used to fit data where fitted pattern is shown by red line).

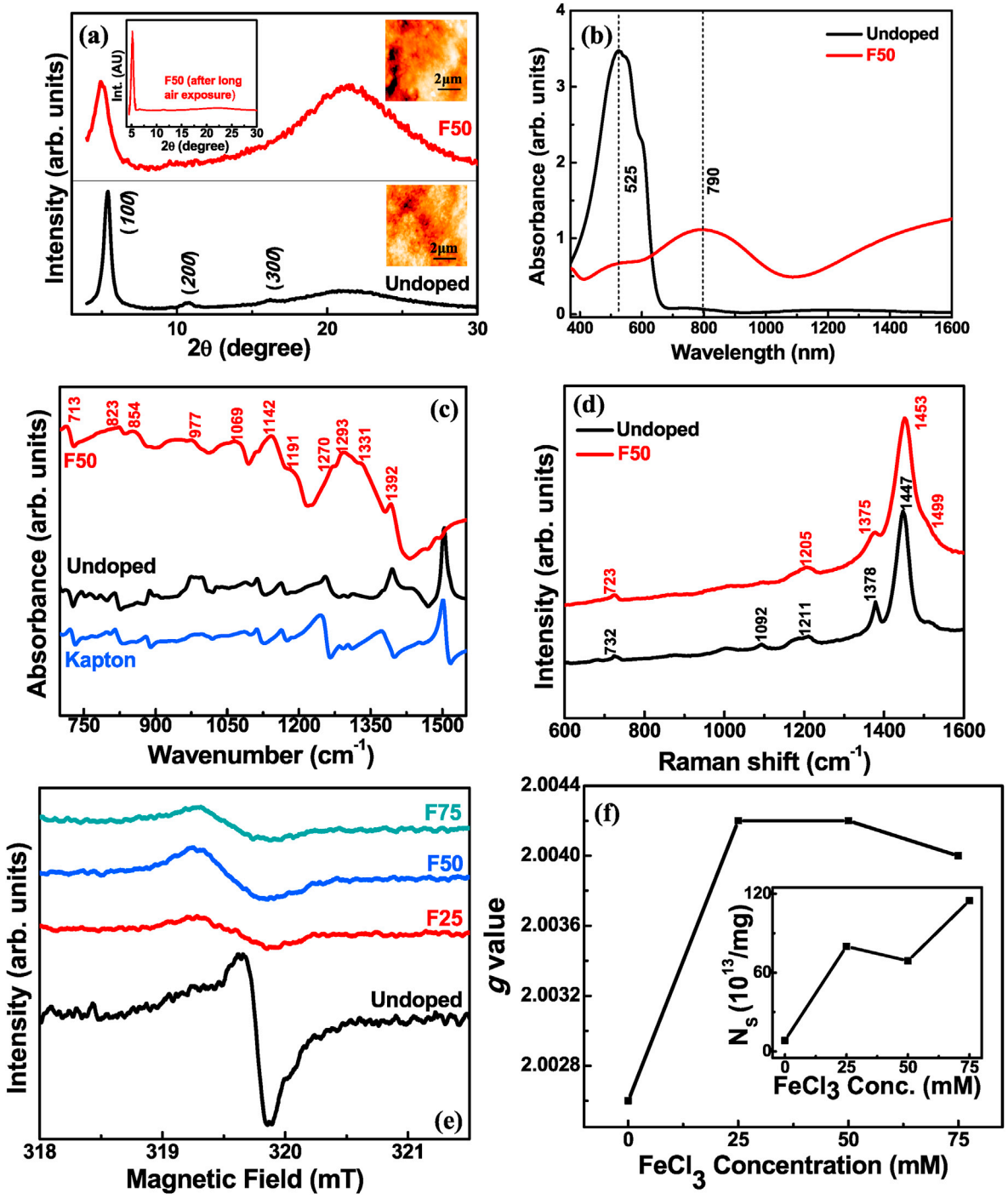

Fig. 4. Results for undoped and F50 films: (a) X-ray diffraction data and AFM images (Inset on the top left shows the XRD of doped films after very long exposure to air); (b) UV-vis-NIR spectra; (c) FTIR spectra; (d) Raman spectra; (e) ESR signal intensity (first derivative) versus Magnetic field; (f) Plot of *g*-factor, and average number of spins (N_s) per unit mass (shown in the inset) versus dopant concentration.

Table 2
Summary of the results obtained from Impedance spectroscopy.

Sample details	C (F)	Re (kΩ)	CPE-e (S-sec)	Ri(kΩ)	CPE-i(S-sec)
Pristine P3HT	9.97×10^{-12}	3.51×10^{3}	1.2×10^{-7}	–	–
Doped P3HT	5.28×10^{-11}	2.72×10^{2}	4.1×10^{-7}	0.52	3.6×10^{-7}

are discussed ahead. FTIR spectra of both the undoped and F50 samples along with that of Kapton substrate (so that signals from the film and the substrate can be differentiated) are shown in Fig. 4(c). Usually, for undoped P3HT sample, the bands at 724 and 821 cm^{-1} are assigned to C-H out-of-plane vibrations while C-H in-plane vibrations appear at 1052 cm^{-1}. The band at 1377 cm^{-1} is attributed to the $-CH_3$ deformational vibration. Whereas, FTIR data of doped samples show the presence of bands at 1392, 1293, 1142, 1069, 977, 854 and 823 cm^{-1} which correspond to the polaron bands [39,40]. For doped F50 sample, the relatively higher intensity of band at 1142 cm^{-1} in comparison to the bands at 1392 cm^{-1} and 1293 cm^{-1} shows that the carriers generated are bipolarons; thus showed consistency with UV-Vis-NIR analysis.

Fig. 4(d) shows the Raman spectra of typical undoped and F50 samples in the region 600-1600 cm^{-1}. The main in-plane skeleton mode assigned to $C_\alpha = C_\beta$ stretching vibration is observed at 1447 cm^{-1} for undoped samples and is blue shifted to 1453 cm^{-1} on doping [39,40]. This blue-shift (1453 cm^{-1}) is quite unusual and can be attributed towards the high frequency of the bipolaron band [39]. Shift of this in-plane mode to higher energies indicates reduced molecular planarity on doping due to intercalation of ions [39]. While, the peak at 1378 cm^{-1} assigned to C_β-C_β (intra-ring) stretching vibration, on doping, got broadened as well as slightly red shifted to 1375 cm^{-1}. Higher width (FWHM) and shifting (blue/red respectively) of both these $C_\alpha = C_\beta$ and C_β-C_β (intra-ring) peaks in case of F50 indicate molecular disorder; and thus, on doping, shows predominance of amorphous structure as already observed by XRD analysis. Doped F50 sample also exhibits similar broadening and shift of peaks for the inter-ring C-C stretching (at 1211 to 1205 cm^{-1}) and C-S-C deformation modes (at 732 to 723 cm^{-1}). Due to red-shifting and peak broadening of C-S-C modes, it can be concluded that the thiophene rings of P3HT got deformed and probably, tensile strain due to dopant inclusions caused conformation to be more linear (*i.e.* quinoid configuration) [34,39].

This stretched conformation supports facile motion of ions/charge carriers as confirmed by the enhanced mobility values obtained for doped films by Hall measurements (given in Table 1). However, it can be concluded that these deformed thiophene rings supporting mobility of ions could obstruct facile movement of polarons and thus, would reduce electronic conductivity. Electron spin resonance technique was used to obtain further insight into mechanism of charge transport in the films. ESR signal as a function of magnetic field is plotted in Fig. 4(e). It is seen that undoped films have relatively sharp peak as compared to doped films, while the peak-broadening increases on doping by $FeCl_3$ which indicates the occurrence of magnetic dipolar interactions between spins of charge carriers generated due to doping [41–43]. In addition, doped films exhibit lower resonance field. Average number of spins/unit mass (N_s) has also been estimated for different films and results are shown in the inset of Fig. 4(f). N_s that was found to increase by about two orders of magnitude on doping, indicates formation of charge carriers i.e. polarons/bipolarons. Spin *g*-factor determined from the resonance field was found to increase from 2.0026 for undoped films to ~2.0042 in case of doped, and shown in Fig. 4(f). Sharp increase in *g*-factor on doping indicates a change in conduction nature. As conduction in undoped films is because of positive carriers (also observed from Seebeck coefficient and Hall Effect measurements), we expect that doping caused formation of negative electronic charge carriers. The enhancement of spin *g*-factor from ~2.002 for positive polarons to ~2.005 for negative polarons as reported for organic semiconductors Th-DTTzTz and 4-CN-Ph-TDTzTz supports above interpretation regarding change of conduction type in our films [44]. The value of *g*-factor was however nearly independent of dopant concentration. In fact, this doping independent behaviour as shown by *g*-value (saturated at 2.0042) also finds agreement with this interpretation; since all the doped samples have similar type of negative electronic charge carriers (in addition to conducting ions), spin-orbit interactions at local site (around) $FeCl_3$ did not get altered much with further change in doping levels and hence, resulted in saturation of *g*-factor that is determined mainly from spin-orbit interactions [43,45]. Further support for *n*-type conduction is provided by work-function mapping data measured by Kelvin probe and shown in Fig. 5.

The undoped and doped films exhibited work functions of ~5.34 and 5.28 eV respectively. Lower value of work function in case of the doped film indicates that Fermi-level got shifted towards the conduction band; thus, confirms the *n*-type doping as expected. Mechanism of doping is further analyzed with the help of XPS measurements and the results are shown in Fig. 6. The survey spectra in Fig. 6(a) show that undoped films exhibited S2p, C1s and O1s peaks while in case of doped samples additional Cl2p and Fe2p peaks were also present. High resolution S2p spectra (shown in Fig. 6(b)) for undoped samples may be deconvoluted into $S2p_{3/2}$ and $S2p_{1/2}$ peaks with binding energies of 163.1 and 164.7 eV respectively; corresponding to S-C bonding in the thiophene ring. By taking the area ratio of C1s and S2p peaks, along with their respective sensitivity factors of 0.296 and 0.666, C/(C + S) ratio for undoped films was estimated as ~0.9; which shows good agreement with the chemical formula ($C_{10}H_{14}S$) of P3HT [46]. In case of doped samples, the S2p spectra exhibited components at higher binding energy values ($S2p_{3/2}$ at 169 eV) that may be attributed to the oxidation of the thiophene units of P3HT by the dopant [47].

High resolution C1s spectra for undoped films shows a broad asymmetric peak in Fig. 6(c), that can be deconvoluted into four components at binding energies of 283.5, 284.8, 286.2, and 288.3 eV respectively. These peaks are respectively assigned to β carbon atoms (*i.e.* next to α carbon), α carbon atoms (*i.e.* C atom with attached C_6H_{13} chain), C-atoms bonded to S-atoms and 'shake-up' line due to aromatic thiophene ring [46,48,49]. Higher binding energy value of 286.2 eV is assigned to C-atoms that are bonded to the S-atoms because more electro-negativity of the S-atom in P3HT withdraws electron density from the adjacent C-atoms [47]. The extinct binding energy peak (at 283.5 eV) in C1s spectrum for the doped F50 films shows that the chemical environments certainly have a predominance of α carbons as compared to β carbons and this finding is in consistence with the results reported in case of higher doping levels [50]. Fe2p spectra of F50 films given in Fig. 6(d) shows that $Fe2p_{3/2}$ peak may be deconvoluted into two components with binding energies of 709.5 and 712.5 eV that are attributed to different oxidation states of Fe [51]. As reported by Tosi et al., it is proposed that dopant $FeCl_3$ forms dimers of Fe_2Cl_6 that partially decompose into $Fe_2Cl_5^+$ and $Fe_2Cl_7^-$ with peaks at 709.5 and 712.5 eV respectively [23]. Based on their findings, we propose that ionic conduction in our films occurs due to movement of Cl^- ions from one Fe_2Cl_6 dimer to nearby neutral dimer leaving behind $(Fe_2Cl_5)^+$ and forming $(Fe_2Cl_7)^-$ as well as through reverse/back transfer of Cl^- from $(Fe_2Cl_7)^-$ to neighbouring Fe_2Cl_6. However, if there occurs such a thermodiffusion of Cl^- in $(Fe_2Cl_5)^+$ and $(Fe_2Cl_7)^-$ ion path, it can cause accumulation of ions near the cold-end to cause charge imbalance across the whole sample. Therefore, to confirm this, a doped sample was subjected to the temperature gradient, and XPS spectra of both the hot- and cold-ends were taken by slicing the sample into two parts. The results shown in Figure S2 of supplementary information reveal a measurable change in the high resolution S2p peak in which the positively charge sulphonate component got enhanced in the hot-end sample in comparison to the cold-end sample. While the high resolution Fe2p peak in Figure S2(b) shows that the relative contribution of high binding energy peak 712eV corresponding to $(Fe_2Cl_5)^+$

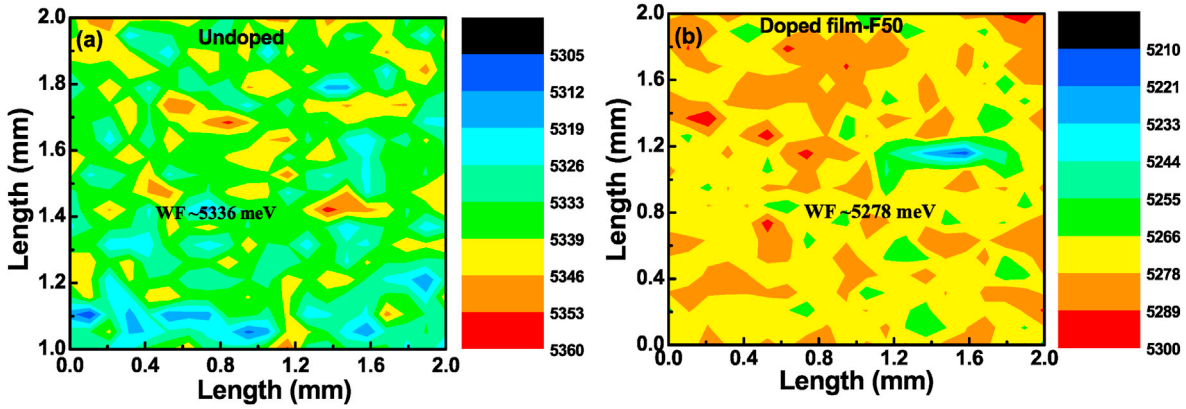

Fig. 5. Work function mapping of P3HT films: (a) Undoped; (b) Doped F50 sample.

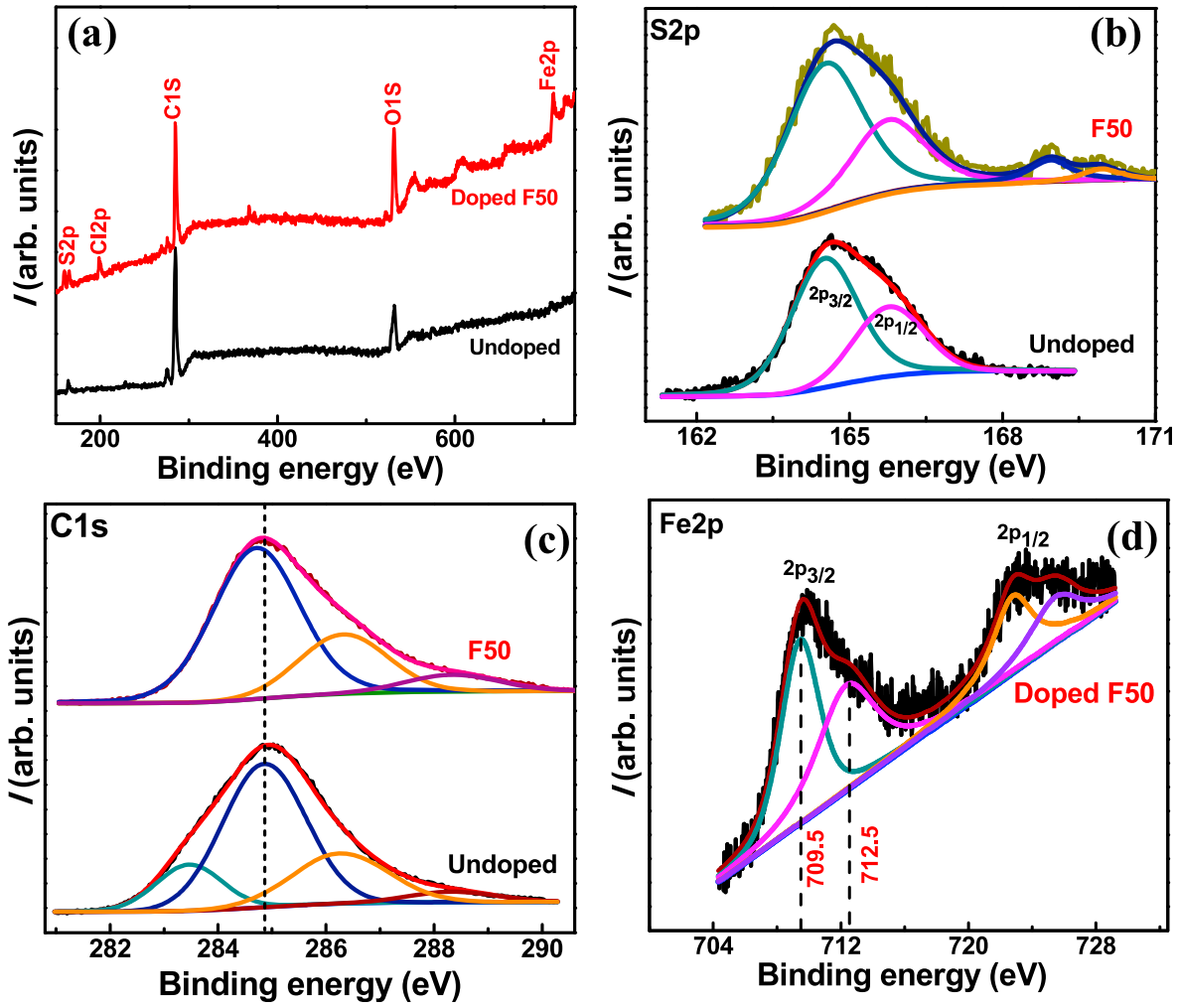

Fig. 6. XPS results for undoped and doped F50 films: (a) Survey spectra; High resolution (b) S2p, (c) C1s, and (d) Fe2p spectra (in doped film only).

enhanced in case of a hot-end sample. The presence of more numbers of chlorine deficient $(Fe_2Cl_5)^+$ species in the hot-end sample confirmed our proposition that there occurred thermo-diffusion of Cl^- ions across the P3HT matrix. Schematic given in Fig. 8(a) shows the proposed mechanism of anionic conduction in case of a doped P3HT matrix. Such movement of Cl^- ions from the hot-end to cold-end also finds support from the work-function mapping data measured using Kelvin probe technology for separate parts of the film (*i.e.* hot- and cold-ends of the film) that were subjected to a temperature gradient for a long time. Fig. 7 depicts that work function of hot- and cold-end of the doped samples is ~5.27 and 5.31 eV respectively, which shows agreement with the assumption that the Cl^- ions moved towards the cold-end. And this movement of ions, hence, resulted in holes' doping (or reduction in electron doping) for maintaining the electrical neutrality.

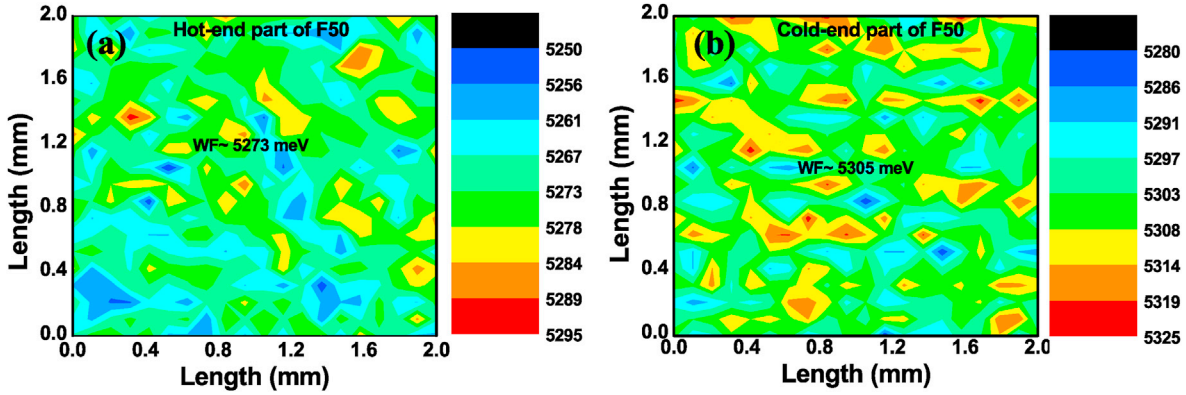

Fig. 7. Work function mapping of P3HT films: (a) Hot-end part; and (b) Cold-end part.

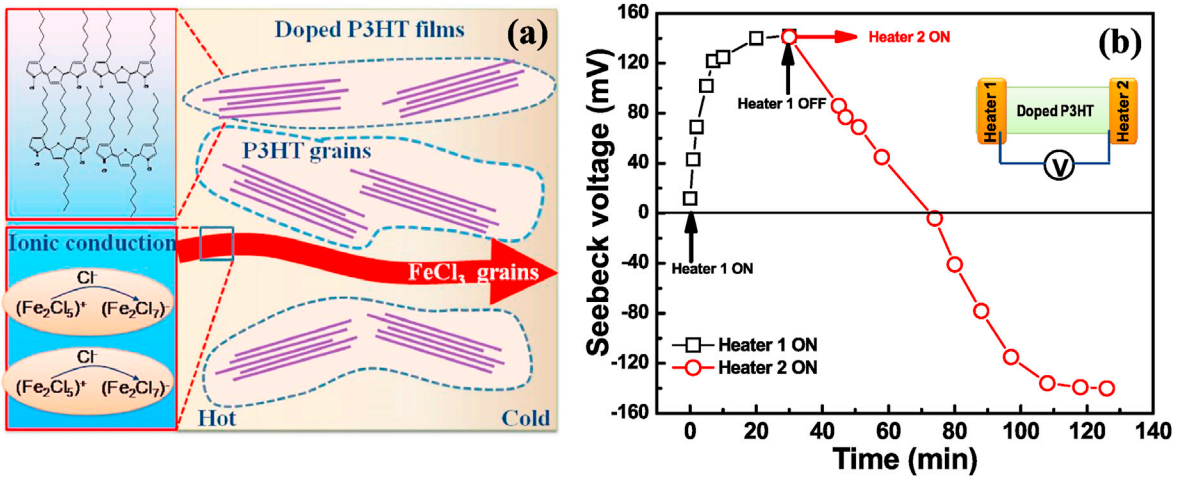

Fig. 8. (a) Schematic showing mechanism of thermodiffusion of Cl^- ions through the P3HT matrix; (b) Seebeck voltage versus time of a single doped film showing regenerative behaviour of Seebeck voltage as observed under See-saw type of arrangement of heater for creating temperature difference.

Furthermore, we like to add that in addition to this anionic movement, the positively charged polarons/bipolarons will also try to move towards the cold-end but the deformed polymer chains along with amorphous nature of doped films will restrict their movement to cold-end. Hence, it can be concluded that a considerable value of electrical conductivity (as confirmed by increase in mobility and carrier concentration values obtained by Hall measurement) and a huge *n*-type Seebeck coefficient that have been achieved in doped P3HT films are mainly due to anionic movement under temperature gradient. To the best of our knowledge, such ionic conduction mediated huge negative Seebeck coefficient has never been observed in P3HT. Perhaps, the electrostatic interaction between mobile chloride ions and immobile polyions reduces the activation energy required for thermodiffusion of anions, and thus, supported facile motion of the anions [16]. Moreover, Seebeck voltage in case of doped P3HT films exhibited regenerative behaviour. In order to confirm this behaviour of Seebeck voltage in case of doped P3HT films exhibiting ionic conduction, we carried out a simple experiment in which two heaters were mounted (as shown in inset of Fig. 8(b)) on both the ends of a doped P3HT film to create temperature difference. At first, only Heater 1 was made ON to create a temperature difference of 45 °C, and it was observed that the obtained open circuit voltage got saturated at 140 mV after a time period of 20 min. After that, Heater 1 was switched off, and Heater 2 was turned ON. From the data shown in Fig. 8(b), it can be easily observed that approximately 45 min are needed to nullify the effect of temperature produced by Heater 1.

Moreover, nearly 30 min are further needed to build up the reverse open circuit voltage of −140 mV. The long duration of time that was required to achieve the saturation of output voltage may be due to low mobility of ions as well as due to the time needed to develop a stable gradient of 45 °C depending upon the thermal mass of heater assembly. In fact, this regenerative behaviour of Seebeck voltage (shown in Fig. 8(b)) confirms that the doped P3HT samples are reusable. It is noteworthy that polyelectrolytes which consist of solvent (mainly water) and salt (for instance as reported by Crispin et al. [10–12]) when subjected to a temperature gradient can exhibit degraded performance since ionic conduction is humidity dependent in their case [15,16]. But $FeCl_3$ doped P3HT polymeric films reported here are humidity independent. It was observed that the change in the conductivity values was not appreciable within the accuracy of ±3%, even when films were measured in two different humidity conditions (*i.e.* 40% and 60%) at room temperature. However, degradation in *n*-type conduction was observed above 70 °C but this degradation is not due to humidity rather can be attributed to the regaining of the crystalline nature of the films which enhances the polaronic conduction resulting in suppression of *n*-type ions-mediated conduction. In fact, it has been observed that the degradation of Seebeck voltage occured only after extended use of samples above 70 °C and was very much

similar to that obtained in case of the samples that were kept in storage for more than 3 months. This also confirms that such degradation occurs due to crystallization as shown by the XRD data (given in Fig. 4) of a sample kept in long time storage.

The environmental stability as well as such a high and regenerative negative Seebeck coefficient, worked as stimuli to investigate the potential of these P3HT films in thermoelectric applications. Therefore, a small prototype thermoelectric power generator was fabricated by connecting seven stripes of F50 films in parallel as shown by the photograph given in the inset of Fig. 9(a). The parallel combination has been adopted to boost the current generation capability of the device. Open-circuit voltage (V_{OC}) of the device was measured as a function of temperature difference (temperature of cold-end was fixed at 24 °C). Notably, at the maximum hot-end temperature (T_h) of 70 °C (*i.e.* for ΔT ~46 °C), the device exhibited V_{OC} of ~128 mV which is consistent with the measured Seebeck coefficient of ~2.7 mV/K in case of individual film/strip. The device could not be heated above 70 °C as on heating at high temperatures ionic conductivity was lost, and device showed hole type conduction with low *p*-type Seebeck coefficient as reported in several studies [18,19,25,26]. Such loss of ionic conductivity is the conventional behaviour that is usually exhibited on crystallization of films [18].

Such degradation of ionic conductivity on crystallization has also been observed for our films/device that have been kept in air for a long period of few months (*i.e.* greater than 3 months), and this fact is confirmed by the XRD shown in the inset of Fig. 4(a) that reveals crystallization in such air-exposed films. Time dependence of V_{OC} given in Fig. 9(b) showed a small decrease by 2.5% over 60 min. To extract power from the device, a matched load of 166 Ω (*i.e.* equivalent to the device resistance at 30 °C) was also connected at the terminals of device. Measured current and power were seen to increase as a function of ΔT as shown in Fig. 9(a&c). The device tested for continuous operation with a fixed load resistance of 166 Ω at T_h = 70 °C showed an initial voltage of 64 mV with a current of ~391 μA. However, estimation of the magnitude of current obtained at matched load has also been done theoretically in order to check that whether such a high current is the result of the ionic movement. For this, we calculated the amount of fraction of chlorine ions that move from hot-end to cold-end in a 2-h period. As current reduces from ~391 μA to nearly zero over a period of 2 h, the total charge flowing through the external circuit is estimated to be ~0.7 C by integration of current versus time curve. As thickness of undoped films is ~10 μm and considering P3HT density equal to 1.1 g/cm^3 as reported in the literature, the film has 6 × 10^{20} Sulphur atoms/cm^2 area. XPS measurements for F50 films show that Fe/S atomic density is 0.39; thus, indicate that there are ~2.4 × 10^{20} Fe atoms/cm^2 in the film. Since the total area of the film used in the device is 7 cm^2, we get total Fe content of ~1.7 × 10^{21} atoms. Considering that one Cl atom per Fe_2Cl_6 dimer may take part in

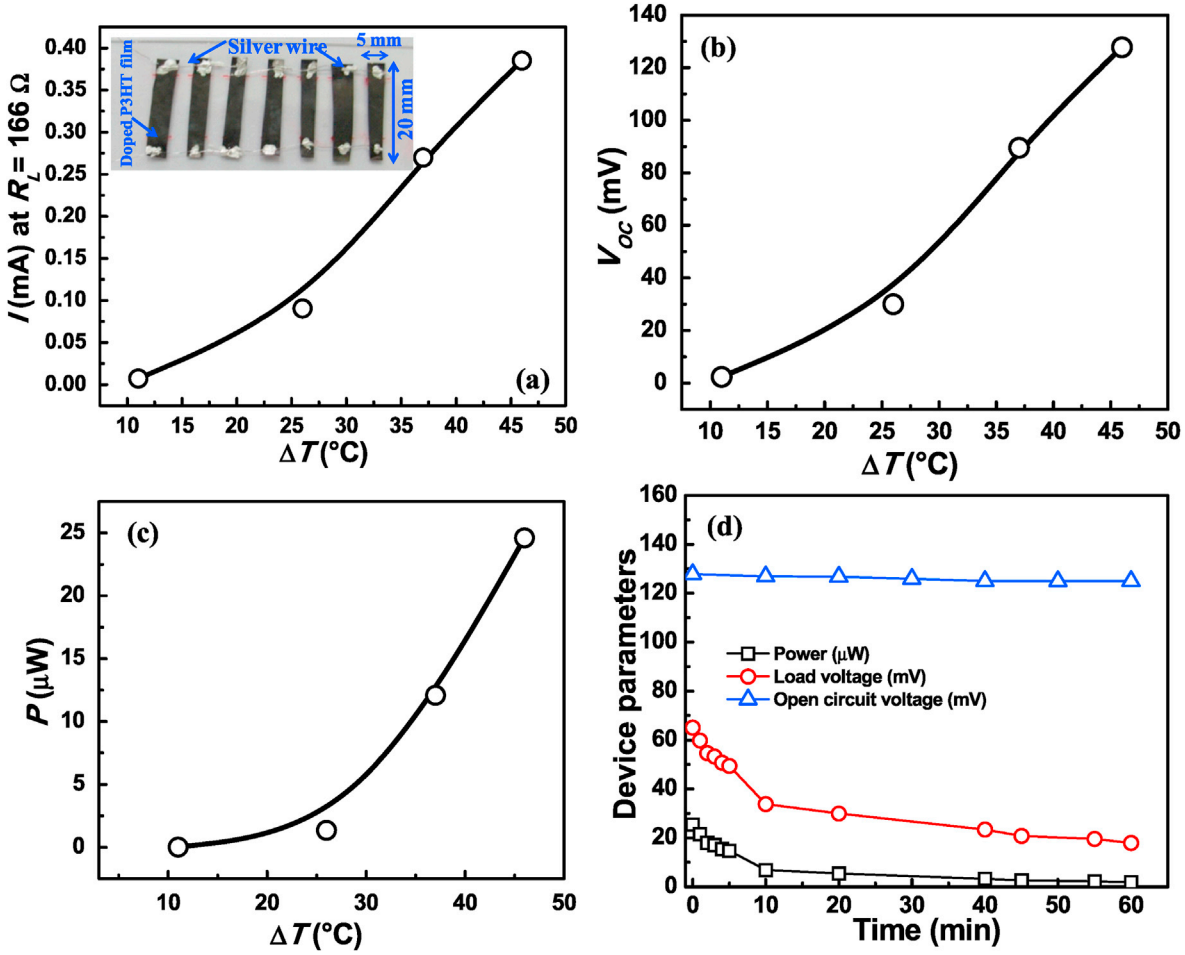

Fig. 9. (a) Current generated by the 7 thermoelements' device at the matched load (equivalent to the device resistance of 166 Ω at 30 °C) and Inset shows the actual photograph of the thermoelectric power generator fabricated using F50 doped films; (b) Open-circuit voltage (V_{OC}) as a function of temperature difference; (c) Power generated by the device at the matched load *i.e.* 166 Ω; (d) Plot showing time dependence of Open-circuit voltage, Load voltage (at 166Ω) and power of the device fabricated using doped films.

Table 3
Comparison of the thermoelectric power generation capability of devices made with various conducting polymer and their composites.

Thermoelements	Device configuration	Output	Ref.
n-TTF-TCNQ/PVC blend *p*-PEDOT-Tos	54 *p*-*n* legs, $\Delta T = 10$ °C,	Power: 0.128 μW Power Density: 0.32 μW/cm^2	52
p-Te nanowire coated with P3HT	Connecting two *p*-type layer in series, $\Delta T = 55$ °C (in series & parallel configuration) Connecting two *p*-type layer in series,	Voltage: 38 mV, Current: 320 nA	53
n-poly[Na_x(Ni-ett)] *p*- poly[Cu_x(Ni-ett)]	35 *p*-*n* legs, $\Delta T = 82$ °C, $T_H = 150$ °C	Voltage: 0.26 V, Current: 10.1 mA, Power: 750 μw Power Density: 1.19 mW/cm^2	54
p-PEDOT:PSS	$\Delta T = 70$ °C 10 windings of 576 junctions (~1m^2) without any adhesive with heater at the centre	Power: 50–60 pW	55
p-PP-PEDOT	$\Delta T = 5.3$ °C	Voltage: 590 μV	56
p-PEDOT:PSS/paper composite	300 pieces of parallel connected paper (10 in parallel, 30 in series, each piece contain 11 PEDOT:PSS arrays), $\Delta T = 100$ °C	Voltage: 40 mV, Power: 50 μW	57
n-poly[K_x(Ni-ett)]/PVDF/DMSO composite *p*-poly[Cu_x(Cu-ett)]/PVDF/DMSO composite	6 p-n legs, $\Delta T = 25$ °C, $T_H = 50$ °C	Voltage: 15 mV, Current: 3 μA, Power: 45 nW, Power Density: 50 μW/cm^2	58
n-Bi_2Te_3/PEDOT: PSS composite *p*-Sb_2Te_3/PEDOT:PSS composite	7 p-n legs at $\Delta T = 50$ °C, $T_H = 60$ °C)	Voltage: 85.2 mV,	59
p-PEDOT:PSS	5 *p* strips at $\Delta T = 75.2$ °C	Voltage: 4.3 mV, Power: 12.29 nW Power Density: 43.1 nW/cm^2	60
n-$Cu_{0.1}Bi_2Se_3$/PVDF composite	$\Delta T = 15$ °C	Voltage: 1.3 mV	61
p-doped polypyrrole free standing	7 stripes (*p*- legs) connected in series, $\Delta T = 80$ °C, $T_H = 70$ °C	Voltage: 336 μV, Current: 46 nA Power: 7.7 pW Power Density: 0.03 μW/cm^2	62
n-doped P3HT free-standing	7 stripes (*n*- legs) connected in parallel, $\Delta T = 46$ °C, $T_H = 70$ °C	Voltage: 128 mV, Current: 391 μA Power: 25 μW Power Density: 6 mW/cm^2	This work
n-doped P3HT free-standing	7 stripes (*n*- legs) connected in series, $\Delta T = 46$ °C, $T_H = 70$ °C	Voltage: 700 mV, Current: 40 μA Power: 14 μW Power Density: 3.28 mW/cm^2	This work

conduction, total charge that may take part in conduction is estimated as = 136 C. It comes out that the charge of 0.7 C that was flowing through external circuit and estimated experimentally from current verses time plot, constituted 0.5% of the total ionic charge (i.e. 136 C estimated theoretically); and conduction of such amount appears reasonable.

Furthermore, Fig. 9(d) reveals that in contrast to time independence of V_{OC} which was quite stable over a time period of 1 h, the output power (as well as the load voltage) significantly reduced with time i.e. from initial value of 25 μW it decreased to 2 μW in an hour (extrapolated current reduced to near zero in about 2 h) as also reported by Crispin et al. in case of polyelectrolytes [16]. Regarding this behaviour, we note that initially due to ionic diffusion, negative charge (due to Cl^- ion movement) gets concentrated at the cold-end which in turn resulted in the accumulation of positive charges at the hot-end. So, when load is connected to the device, electrons flowing through the external circuit neutralize the accumulated ions at the ends. Therefore, the power/load voltage reduces probably because of the two reasons: (a) the movement of the electrons through the external circuit neutralizes the ionic charge much faster than their separation by continued ionic movement; and (b) as more and more Cl^- ions move towards the cold-end, the changed concentration gradient reduces further movement of the ions.

However, the device connected in the series configuration delivered $V_{OC} = 700$ mV and $I_{SC} = 40$ μA. This may be compared to expected values of $V_{OC} = 130 \times 7 = 910$ mV, and $I_{SC} = 111$ μA calculated as 1/7th of the short-circuit current of seven devices in parallel. The observed open circuit voltage of 700 mV in case of series connection of films was less than the expected value of 910 mV perhaps due to loss of thermal gradient. Since the wires that were used to connect hot-end of the film with the cold-end of the next one might have conducted some heat resulting in lowering the temperature difference across the sample. Whereas, the short circuit current is found less than the expected value because of two reasons: (i) reduced temperature difference, and (ii) short circuit current of the devices in series is controlled by the device having its minimum value. It can be seen from Fig. 9(a) in which actual photograph of the 7 films shows that width of samples is not same; and short circuit current being proportional to width for devices in series is therefore, expected to be controlled by the sample with minimum width. Comparison of the thermoelectric power generation capability of P3HT films reported in this work with other conducting polymers and their composites has been summarized in Table 3. It can be seen that power generation capability of thin film devices reported here compares well with other reported devices [52–62]. Moreover, it is emphasized that the thermoelectric power generator fabricated in this work consists of only 7 stripes (*n*-legs), and when placed under a temperature difference of 46 °C, it exhibited much better voltage/current/power in comparison to the other reported devices under similar conditions.

4. Conclusion

The present work focusses on revealing the role of ionic contribution in conduction mechanism. Doping of ferric chloride in poly(3-hexylthiophene) (P3HT) films not only caused transition in conduction nature from *p*-to *n*-type but also peeled-off the films

from the substrates to result in a free-standing motif. Negative Cl^- ions of dopant $FeCl_3$ generated a very large *n*-type Seebeck coefficient (−2.7 mV/K at 70 °C) which suggests that these films can fill the gap for a stable and reliable *n*-type polymer that is much needed in the organic thermoelectric domain. Impedance spectroscopy studies confirmed the predominance of ionic conduction (~500 times more than electronic conduction) in the films; which is further supported by the results of many characterization techniques. The dominance of ionic conduction is also reflected by the amorphous structure of P3HT films (as revealed by FTIR and Raman analysis) since such type of structure can minimize the electronic conduction. In pursuit of the practical use of these free-standing films, a prototype device was fabricated that delivered an open-circuit voltage of 130 mV; and on applying load, a current of ~391 μA was obtained for a temperature difference of 46 °C. Measured voltage under open-circuit conditions was found to be quite stable (reducing by 2.5% over 1 h) while current under load reduced to about 25% of initial value in 1 h. In short, the rare *n*-type behaviour can be obtained, and thermo-diffusion of anions in such free-standing P3HT films not only generates huge Seebeck coefficients useful for intermittent heat conversion but can also be utilized for charging of supercapacitors to power other devices later on. Moreover, such a strategy of utilizing ionic transport to dramatically improve Seebeck coefficient reveals that ionic conduction can be channelized along with electronic transport to use such polymeric films in the devices that require both types of transport.

Author contributions

M. Bharti designed and executed all the experiments. A. Singh analyzed all the characterization results and proposed the mechanism of charge transport. Also, the lab made set-up for measurement of electrical conductivity and Seebeck coefficient was designed and developed by him. A. K. Debnath is responsible for carrying out all the experiments regarding X-ray photoelectron spectroscopy and analysis of XPS results. A. K. Chauhan did Raman analysis and AFM studies. K. P. Muthe helped in editing the manuscript. S. K. Gupta verified and supervised all the obtained results. He also wrote some portion of Results and discussion section. K. Marumoto analyzed all the ESR results. T. Mori discussed the results and helped in writing a part of the manuscript. D. K. Aswal supervised the entire research work. All the experiments were performed under his guidance. All the authors discussed the results and M. Bharti and A. Singh prepared the manuscript.

Declaration of competing interest

The authors declare that they have no known competing financial interests or personal relationships that could have appeared to influence the work reported in this paper.

Acknowledgements

The authors also wish to express their sincere thanks to Dr. Sanjay Kumar, Dr. Manoranjan Ghosh and Dr. Shiv Govind of BARC, for their support in providing Raman, Hall measurement and XRD data of the samples. TM thanks support from JST Mirai JPMJMI19A1.

Appendix A. Supplementary data

Supplementary data to this article can be found online at https://doi.org/10.1016/j.mtphys.2020.100307.

References

[1] T. Mori, S. Priya, Materials for energy harvesting: at the forefront of a new wave, MRS Bull. 43 (2018) 176–180.
[2] Z. Soleimani, S. Zoras, B. Ceranic, S. Shahzad, Y. Cui, A review on recent developments of thermoelectric materials for room-temperature applications, Sustain. Energy Technol. Assess. 37 (2020) 100604.
[3] I. Petsagkourakis, K. Tybrandt, X. Crispin, I. Ohkubo, N. Satoh, T. Mori, Thermoelectric materials and applications for energy harvesting power generation, Sci. Technol. Adv. Mater. 19 (2018) 836–862.
[4] M. He, F. Qiu, Z. Lin, Towards high-performance polymer based thermoelectric materials, Energy Environ. Sci. 6 (2013) 1352–1361.
[5] R. Kroon, D.A. Mengistie, D. Kiefer, J. Hynynen, J.D. Ryan, L. Yu, C. Muller, Thermoelectric plastics: from design to synthesis, processing and structure–property relationships, Chem. Soc. Rev. 45 (2016) 6147–6164.
[6] O. Bubnova, X. Crispin, Towards polymer-based organic thermoelectric generators, Energy Environ. Sci. 5 (2012) 9345–9362.
[7] M. Bharti, A. Singh, S. Samanta, D.K. Aswal, Conductive polymers for thermoelectric power generation, Prog. Mater. Sci. 93 (2018) 270–310.
[8] N. Nandihalli, C.J. Liu, T. Mori, Polymer based thermoelectric nanocomposite materials and devices: fabrication and characteristics, Nano Energy 78 (2020) 105186.
[9] D.K. Aswal, R. Basu, A. Singh, Key issues in development of thermoelectric power generators: high figure-of-merit materials and their highly conducting interfaces with metallic interconnects, Energy Convers. Manag. 114 (2016) 50–67.
[10] D. Zhao, S. Fabiano, M. Berggren, X. Crispin, Ionic thermoelectric gating organic transistors, Nat. Commun. 8 (2017) 14214–14218.
[11] F. Jiao, A. Naderi, D. Zhao, J. Schlueter, M. Shahi, J. Sundstrom, H. Granberg, J. Edberg, U. Ail, J. Brill, T. Lindstrom, M. Berggren, X. Crispin, Ionic thermoelectric paper, J. Mater. Chem. A 5 (2017) 16883–16888.
[12] H. Wang, U. Ail, R. Gabrielsson, M. Berggren, X. Crispin, Ionic Seebeck effect in conducting polymers, Adv. Energy Mater. 5 (2015) 1500044–1500046.
[13] K. Choi, S.L. Kim, S.-I. Yi, J.-H. Hsu, C. Yu, Promoting dual electronic and ionic transport in PEDOT by embedding carbon nanotubes for large thermoelectric responses, ACS Appl. Mater. Interfaces 10 (2018) 23891–23899.
[14] X. Guan, H. Cheng, J. Ouyang, Significant enhancement in the Seebeck coefficient and power factor of thermoelectric polymers by the Soret effect of polyelectrolytes, J. Mater. Chem. A 6 (2018) 19347–19352.
[15] D. Zhao, A. Martinelli, A. Willfahrt, T. Fischer, D. Bernin, Z.U. Khan, M. Shahi, J. Brill, M.P. Jonsson, S. Fabiano, X. Crispin, Polymer gels with tunable ionic Seebeck coefficient for ultra-sensitive printed thermopiles, Nat. Commun. 10 (2019) 1093.
[16] H. Wang, D. Zhao, Z.U. Khan, S. Puzinas, M.P. Jonsson, M. Berggren, X. Crispin, Ionic thermoelectric figure of merit for charging of supercapacitors, Adv. Electron. Mater. 1700013 (1–6) (2017).
[17] B. Endrdi, J. Mellar, Z. Gingl, C. Visy, C. Janaky, Molecular and supramolecular parameters dictating the thermoelectric performance of conducting polymers: a case study using poly(3-alkylthiophene), J. Phys. Chem. C 119 (2015) 8472–8479.
[18] Y. Xuan, X. Liu, S. Desbief, P. Leclere, M. Fahlman, R. Lazzaroni, M. Berggren, J. Cornil, D. Emin, X. Crispin, Thermoelectric properties of conducting polymers: the case of poly(3-hexylthiophene), Phys. Rev. B 82 (2010) 115454–115459.
[19] Q. Zhang, Y. Sun, W. Xu, D. Zhu, Thermoelectric energy from flexible P3HT films doped with a ferric salt of triflimide anions, Energy Environ. Sci. 5 (2012) 9639–9644.
[20] M. He, J. Ge, Z. Lin, X. Feng, X. Wang, H. Lu, Y. Yang, F. Qiu, Thermopower enhancement in conducting polymer nanocomposites via carrier energy scattering at the organic–inorganic semiconductor interface, Energy Environ. Sci. 5 (2012) 8351–8358.
[21] W. Lee, C.T. Hong, O.H. Kwon, Y. Yoo, Y.H. Kang, J.Y. Lee, S.Y. Cho, K.-S. Jang, Enhanced thermoelectric performance of bar-coated SWCNT/P3HT thin films, ACS Appl. Mater. Interfaces 7 (2015) 6550–6556.
[22] C. Bounioux, D.C. Pablo, C.Q. Mariano, S.-G. Marisol, A.R. Goni, Y.R. Rachel, C. Muller, Thermoelectric composites of poly(3-hexylthiophene) and carbon nanotubes with a large power factor, Energy Environ. Sci. 6 (2013) 918–925.
[23] Z. Akdeniz, M.P. Tosi, Ionic conduction and molecular structure of molten $FeCl_3$, Z. Naturforsch. 53a (1998) 960–962.
[24] J. Rivnay, S. Inal, B.A. Collins, M. Sessolo, E. Stavrinidou, X. Strakosas, C. Tasson, D.M. Delongchamp, G.G. Malliaras, Structural control of mixed ionic and electronic transport in conducting polymers, Nat. Commun. 7 (2016) 11287–11295.
[25] B. Endrodi, J. Mellar, Z. Gingl, C. Visya, C. Janaky, Reasons behind the improved thermoelectric properties of poly(3-hexylthiophene) nanofiber networks, RSC Adv. 4 (2014) 55328–55333.
[26] L. Xu, Y. Liu, B. Chen, C. Zhao, K. Lu, Enhancement in thermoelectric properties using a P-type and N-type thin-film device structure, Polym. Compos. 34 (2013) 1728–1734.
[27] J. Hynynen, D. Keifer, C. Muller, Influence of crystallinity on the thermoelectric power factor of P3HT vapour-doped with F4TCNQ, RSC Adv. 8 (2018) 1593–1599.
[28] J. Hynynen, E. Jarswall, R. Kroon, Y. Zhang, S. Barlow, S.R. Marder, M. Kemerink, A. Lund, C. Muller, Enhanced thermoelectric power factor of

tensile drawn poly(3-hexylthiophene), ACS Macro Lett. 8 (2019) 70–76.
[29] A.K. Chauhan, S.K. Gupta, D. Taguchi, T. Manaka, P. Jha, P. Veerender, C. Sridevi, S.P. Koiry, S.C. Gadkari, M. Iwamoto, Enhancement of the carrier mobility of conducting polymers by formation of their graphene composites, RSC Adv. 7 (2017) 11913–11920.
[30] J.R. Macdonalds, D.R. Franceschetti, Impedance Spectroscopy Emphasizing Solid Materials and Systems, Wiley, New York, 1987.
[31] A.E. Javier, S.N. Patl, D.T. Hallinan Jr., V. Srinivasan, N.P. Balsara, Simultaneous electronic and ionic conduction in a block copolymer: application in lithium battery electrodes, Angew. Chem. Int. Ed. 50 (2011) 9848–9851.
[32] R.A. Huggins, Simple method to determine electronic and ionic components of the conductivity in mixed conductors: a review, Ionics 8 (2002) 300–313.
[33] R.K. Singh, J. Kumar, R. Singh, R. Kant, R.C. Rastogi, S. Chand, V. Kumar, Structure–conductivity correlation in ferric chloride-doped poly(3-hexylthiophene), New J. Phys. 8 (2006) 112.
[34] M. Brinkmann, Structure and morphology control in thin films of regioregular poly(3-hexylthiophene), J. Polym. Sci., Polym. Phys. Ed. 49 (2011) 1218–1233.
[35] B.S. Ong, Y. Wu, P. Liu, S. Gardner, High performance semiconducting polythiophenes for organic thin films transistors, J. Am. Chem. Soc. 126 (2004) 3378–3379.
[36] C.Y. Yang, C. Soci, D. Moses, A.J. Heeger, Aligned rrP3HT film: structural order and transport properties, Synth. Met. 155 (2005) 639–642.
[37] E. Lim, K.A. Peterson, G.M. Su, M.L. Chabinyc, Thermoelectric properties of poly(3-hexylthiophene) (P3HT) doped with 2,3,5,6-Tetrafluoro-7,7,8,8-tetracyanoquinodimethane (F4TCNQ) by vapor-phase infiltration, Chem. Mater. 30 (2018) 998–1010.
[38] Y. Prakash, H. Somashekarappa, A. Manjunath, Mahadevaiah, R. Somashekar, Physico-mechanical, AC-conductivity and microstructural properties of $FeCl_3$ doped HPMC polymer films, Adv. Mater. Res. (Techno Press) 2 (1) (2013) 37–49.
[39] J. Yamamoto, Y. Furukawa, Electronic and vibrational spectra of positive polarons and bipolarons in regioregular poly(3-hexylthiophene) doped with ferric chloride, J. Phys. Chem. B 119 (2015) 4788–4794.
[40] R.K. Singh, J. Kumar, R. Singh, R. Kant, S. Chand, V. Kumar, Micromorphology, photophysical and electrical properties of pristine and ferric chloride doped poly(3-hexylthiophene) films, Mater. Chem. Phys. 104 (2007) 390–396.
[41] S. Tanaka, S. Khadijah, Binti Rosli, K. Takada, N. Taniai, T. Yoshitomi, H. Ando, M. Kouichi, Effects of bromination of poly(3-hexylthiophene) on the performance of bulk heterojunction solar cells, RSC Adv. 7 (2017) 46874–46880.
[42] J. Niklas, K.L. Mardis, B.P. Banks, G.M. Grooms, A. Sperlich, V. Dyakonov, S. Beaupre, M. Leclerc, T. Xu, L. Yu, et al., Highly-efficient charge separation and polaron delocalization in polymer–fullerene bulk-heterojunctions: a comparative multi-frequency EPR and DFT study, Phys. Chem. Chem. Phys. 15 (2013) 9562–9574.
[43] F.J. Dyson, Electron spin resonance absorption in metals. II. Theory of electron diffusion and the skin effect, Phys. Rev. 98 (2) (1955) 349.
[44] Y. Ling, S.V. Mierloo, A. Schnegg, M. Fehr, P. Adriaensens, L. Lutsen, D. Vanderzande, W. Maes, E. Goovaerts, S.V. Doorslaer, Electronic structure of positive and negative polarons in functionalized dithienylthiazolo-[5,4-d] thiazoles: a combined EPR and DFT study, Phys. Chem. Chem. Phys. 16 (2014) 10032–10040.
[45] V. Dyakonov, G. Zoriniants, M. Scharber, C.J. Brabec, R.A.J. Janssen, J.C. Hummelen, N.S. Sariciftci, Photoinduced charge carriers in conjugated polymer–fullerene composites studied with light-induced electron-spin resonance, Phys. Rev. B 59 (1999) 8019.
[46] G. Beamson, D. Briggs, High Resolution XPS of Organic Polymers, The Scienta ESCA300 Database John Wiley, Chichester England, 1992.
[47] C.D. Wagner, W.M. Riggs, L.E. Davis, J.F. Moulder, G.E. Muilenberg, Handbook of X-Ray Photoelectron Spectroscopy, Perkin-Elmer Corporation Physical Electronics Division, Eden Prairie, Minnesota, USA), 1979.
[48] J. Heeg, C. Kramer, M. Wolter, S. Michaleis, W. Plieth, W.J. Fisher, Polythiophene-O_3 surface reactions studied by XPS, Appl. Surf. Sci. 180 (2001) 36–41.
[49] J.L. Jenkins, P.A. Lee, K.W. Nebesny, A.L. Ratcliff, Systematic electrochemical oxidative doping of P3HT to probe interfacial charge transfer across polymer–fullerene interfaces, J. Mater. Chem. A 2 (2014) 19221–19231.
[50] A. Singh, Z. Salmi, N. Joshi, P. Jha, P. Decorse, H. Lecoq, S. Lau-Truong, M. Jouini, D.K. Aswal, M.M. Chehimi, Electrochemical investigation of free-standing polypyrrole–silver nanocomposite films: a substrate free electrode material for supercapacitors, RSC Adv. 3 (2013) 24567–24575.
[51] A.P. Grosvenor, B.A. Kobe, M.C. Biesinger, N.S. Mclntyre, Investigation of multiplet splitting of Fe 2p XPS spectra and bonding in iron compounds, Surf. Interface Anal. 36 (2004) 1564–1574.
[52] O. Bubnova, Z.U. Khan, A. Malti, S. Braun, M. Fahlman, M. Berggren, X. Crispin, Optimization of the thermoelectric figure of merit in the conducting polymer poly(3,4-ethylenedioxythiophene), Nat. Mater. 10 (2011) 429–433.
[53] Y. Yang, Z.-H. Lin, T. Hou, F. Zhang, Z.L. Wang, Nanowire-composite based flexible thermoelectric nanogenerators and self-powered temperature sensors, Nano Res 5 (2012) 888–895.
[54] Y. Sun, P. Sheng, C. Di, F. Jiao, W. Xu, D. Qiu, D. Zhu, Organic thermoelectric materials and devices based on p- and n-type poly(metal 1,1,2,2-ethenetetrathiolate)s, Adv. Mater. 24 (2012) 932–937.
[55] R.R. Søndergaard, M. Hosel, N. Espinosa, M. Jørgensen, F.C. Krebs, Practical evaluation of organic polymer thermoelectrics by large-area R2R processing on flexible substrates, Energy Sci. Eng. 1 (2013) 81–88.
[56] T. Park, C. Park, B. Kim, H. Shin, E. Kim, Flexible PEDOT electrodes with large thermoelectric power factors to generate electricity by the touch of fingertips, Energy Environ. Sci. 6 (2013) 788–792.
[57] Q. Wei, M. Mukaida, K. Kirihara, Y. Naitoh, T. Ishida, Polymer thermoelectric modules screen-printed on paper, RSC Adv. 4 (2014) 28802–28806.
[58] F. Jiao, C. Di, Y. Sun, P. Sheng, W. Xu, D. Zhu, Inkjet-printed flexible organic thin-film thermoelectric devices based on p- and n-type poly(metal 1,1,2,2-ethenetetrathiolate)s/polymer composites through ball-milling, Phil. Trans. Roy. Soc. A 372 (2013): 0008.
[59] J.H. We, S.J. Kim, B.J. Cho, Hybrid composite of screen-printed inorganic thermoelectric film and organic conducting polymer for flexible thermoelectric power generator, Energy 73 (2014) 506–512.
[60] Y. Du, K. Cai, S. Chen, H. Wang, S.Z. Shen, R. Donelson, T. Lin, Thermoelectric fabrics: toward power generating clothing, Sci. Rep. 5 (2015): 06411.
[61] C. Dun, C.A. Hewitt, H. Huang, J. Xu, C. Zhou, W. Huang, Y. Cui, W. Zhou, Q. Jiang, D.L. Carroll, Flexible n-type thermoelectric films based on Cu-doped Bi_2Se_3 nanoplate and Polyvinylidene Fluoride composite with decoupled Seebeck coefficient and electrical conductivity, Nano Energy 18 (2015) 306–314.
[62] M. Bharti, P. Jha, A. Singh, A.K. Chauhan, S. Misra, M. Yamazoe, A.K. Debnath, K. Marumoto, K.P. Muthe, D.K. Aswal, Scalable free-standing polypyrrole films for wrist-band type flexible thermoelectric power generator, Energy 176 (2019) 853–860.